Measurement of in-plane thermal diffusivity of solids moving at constant velocity using laser spot infrared thermography

A. Bedoya[1,2], J. González[1,3], J. Rodríguez-Aseguinolaza[1], A. Mendioroz[1], A. Sommier[4], J.C. Batsale[4], C. Pradere[4] and A. Salazar[1,*]

[1]Departamento de Física Aplicada I, Escuela de Ingeniería de Bilbao, Universidad del País Vasco UPV/EHU, Plaza Ingeniero Torres Quevedo 1, 48013 Bilbao, Spain.

[2]Instituto Politécnico Nacional (IPN), Centro de Investigación en Ciencia Aplicada y Tecnología Avanzada (CICATA), Unidad Legaria, Legaria 694, Col. Irrigación, C.P. 11500, Ciudad de México, Mexico.

[3]Department of Applied Physics, CINVESTAV Unidad Mérida, carretera Antigua a Progreso km 6, A.P. 73 Cordemex, Mérida Yucatán 97310, Mexico.

[4]I2M-TREFLE, UMR CNRS 5295, Esplanade des Arts et Métiers 33405 Talence Cedex, France.

*Corresponding author, E-mail address: agustin.salazar@ehu.es

Abstract

In this work, an infrared thermography setup is proposed to measure the in-plane thermal diffusivity of (an)isotropic samples that are moving at constant velocity, as it is the case of in-line production or in-line quality control processes in factories. The experiment consists in heating the moving sample with a focused laser spot, which remains at rest, and recording the surface temperature by an infrared camera. An analytical expression for the surface temperature of the moving sample has been obtained. By analyzing the surface temperature in logarithmic scale, three simple linear relations are obtained, whose slopes give the thermal diffusivity in the direction of the sample movement and in the perpendicular direction. These three linear methods, which are not disturbed by heat losses by convection and radiation, are valid for both opaque and semitransparent samples. Measurements performed on calibrated samples confirm the validity of the methods, which are also valid when the sample is at rest and the laser spot scans its surface at constant velocity, the so-called "flying spot" technique.

Keywords: infrared thermography, flying spot, thermal diffusivity, nondestructive evaluation.

1. Introduction

Heat propagation in steady-state conditions is governed by thermal conductivity, whereas dynamic situations are described by thermal diffusivity, which measures the speed of propagation of heat inside a material during changes of temperature with time [1]. Accordingly, the precise knowledge of the thermal diffusivity of materials is crucial in understanding dynamic processes in thermal engineering. During the last decades, many experimental setups have been proposed to measure the thermal diffusivity of a wide variety of materials and shapes: bulk, thin films on substrate, free-standing films, filaments, etc. (see Ref. (2) for a recent review). In all these setups, the specimen under study remains at rest.

In this work, we propose, using infrared (IR) thermography, to measure the in-plane thermal diffusivity of (an)isotropic samples that are moving at constant velocity. This mimics the real case of in-line production or in-line quality control processes in factories, where heterogeneities, i.e. local changes in the properties, must be detected in real time, without stopping the production chain. In this configuration, the sample surface is heated by a focused CW laser beam while the surface temperature is recorded by an IR video camera. We have obtained an analytical expression for the surface temperature field of the moving sample. By analyzing this temperature distribution in natural logarithmic scale, three simple linear relations are found, from which the thermal diffusivity can be obtained in a straightforward way, i.e. avoiding delicate multiparametric fittings.

To check the ability of the three methods to measure the in-plane thermal diffusivity of moving samples we have performed measurements on calibrated samples covering a wide range of thermal diffusivities (from insulators to good thermal conductors).

It is worth noting that these methods can be directly applied when the sample remains at rest and the laser spot scans the sample at constant velocity. This configuration, known as Flying Spot infrared thermography, was proposed by Kubiak [3] and has been developed by several research groups to detect cracks in a fast manner [4-11].

2. Theory

Let us start considering an anisotropic sample illuminated by an extremely brief (Dirac) pulse laser of energy Q_o and Gaussian profile of radius a (at $1/e^2$). We make the Cartesian reference frame coincide with the principal axes of this anisotropic slab. We consider heat

losses by convection and radiation from the sample surface. The surface temperature rise above the ambient is given by [12]

$$T(x,y,0,t)=\frac{2Q_o\eta}{\pi}A(t)\frac{e^{-\frac{2x^2}{a^2+8D_xt}}}{\sqrt{a^2+8D_xt}}\frac{e^{-\frac{2y^2}{a^2+8D_yt}}}{\sqrt{a^2+8D_yt}}, \tag{1}$$

where $A(t)$ takes the following values depending on the optical properties and thickness of the sample:

(a) For an opaque and thick material $A(t)=\frac{1}{\varepsilon_z}\left[\frac{1}{\sqrt{\pi t}}-\frac{h}{\varepsilon_z}e^{(h/\varepsilon_z)^2t}Erfc\left(\frac{h}{\varepsilon_z}\sqrt{t}\right)\right]$. (2a)

(b) For an opaque and thin material $A(t)=\frac{1}{\rho cL}e^{-\frac{2ht}{\rho cL}}$. (2b)

(c) For a semitransparent and thick material $A(t)=\frac{1}{\rho c}\frac{\alpha\gamma}{\alpha+\gamma}$. (2c)

Here η is the energy fraction absorbed by the sample, α is the optical absorption coefficient of the sample at the laser wavelength, γ is the effective absorption coefficient to the detected IR wavelengths (3 to 5 μm), D is the thermal diffusivity, ε is the thermal effusivity, ρ is the density, c is the specific heat and L is the thickness. We assume that the surface temperature rise is small, so the heat rate dissipated from the surface can be considered as a linear function of the temperature, where h is the linear coefficient of heat losses. Subscripts x,y,z stand for the thermal properties along the principal axes.

Now we consider the same anisotropic sample moving to the right along the x-axis at constant velocity v, while a CW laser of power P_o and Gaussian profile of radius a (at $1/e^2$) remains at rest, as it is shown in Fig. 1. The laser is switched on at $t = 0$. The surface temperature at time t is given by the convolution integral of Eq. (1)

$$T(x,y,0,t)=\frac{2P_o\eta}{\pi}\int_0^t A(t-\tau)\frac{e^{-\frac{2[x-v(t-\tau)]^2}{a^2+8D_x(t-\tau)}}}{\sqrt{a^2+8D_x(t-\tau)}}\frac{e^{-\frac{2y^2}{a^2+8D_y(t-\tau)}}}{\sqrt{a^2+8D_y(t-\tau)}}d\tau\,. \tag{3}$$

Note that at this point we have not established yet the meaning of thermally thick and thin in the case of a moving sample. This point will be clarified at the end of section 3.1.

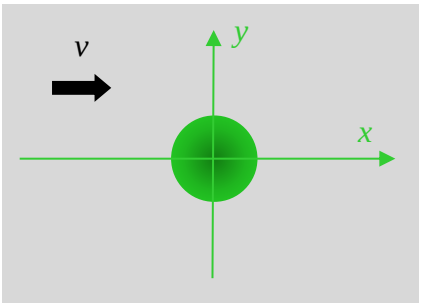

Fig. 1. Front surface of an anisotropic sample moving to the right at constant speed v, while the laser spot is at rest.

3. Three methods to measure the thermal diffusivity

In this section we are proposing three methods to measure the thermal diffusivity of a sample that is moving at constant velocity, by analysing the surface temperature in logarithmic scale. The three methods are valid once the steady-state has been established. The solution of the surface temperature field obtained from the convolution integral Eq. (3) permits a precise determination of the time needed to attain a thermal steady-state, t_c, as a function of the sample velocity. This is calculated as follows: for a given pair of v and D values we calculate the surface temperature for increasing times until the difference with respect to infinite time is smaller than 0.1%. These calculations are performed for a circle of 1 cm of radius around the laser spot. This is due to the fact that the field of view of our IR camera with a microscope lens is around 1 cm × 0.8 mm (see Section 4). Actually, t_c increases as the area that is monitored is enlarged. Figure 2 shows the values of t_c versus the sample velocity calculated for four materials covering a wide range of thermal diffusivities, from thermal insulators (D = 0.1 mm^2/s) to good thermal conductors (D = 100 mm^2/s), using a = 0.1 mm and h = 0. As can be observed, this critical time decreases as the sample velocity rises and as the thermal diffusivity decreases. As these methods are addressed to study large surfaces in short times, we employ velocities $v \geq 2$ cm/s. For these velocities, the steady-state is reached in a few seconds, even for the most conducting samples.

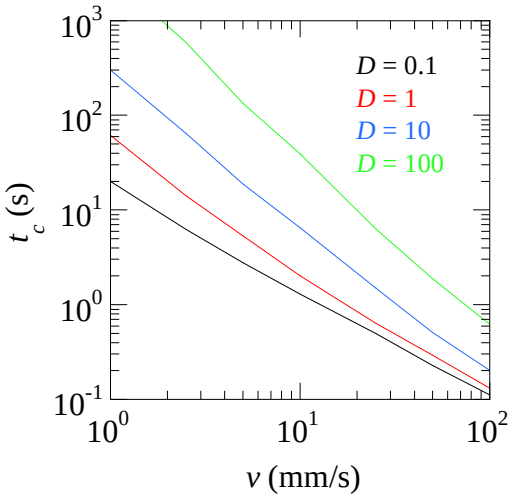

Fig. 2. Calculations of the time needed by the sample to reach the steady-state, t_c, as a function of the sample velocity. Four materials, whose thermal diffusivity is given in mm^2/s, are studied.

Next, we present calculations of the surface temperature field when the steady-state has been stablished. We show in Fig. 3a the isotherms of Ln(T) for an anisotropic sample (D_x = 4 mm^2/s, D_y = 1 mm^2/s, ε_z = 3000 $Ws^{0.5}m^{-2}K^{-1}$) moving to the right at v = 2 cm/s. The sample is heated by a 1 W laser beam of radius a = 0.2 mm, which remains at rest. Calculations are performed for negligible heat losses (h = 0). In Fig. 3b we show the transverse profiles of Ln(T) at different longitudinal distances from the laser spot. As can be observed, the central profile (x = 0) is almost linear, but the shape changes as x increases, in such a way that the transverse profiles become parabolas at long distances from the laser spot. Finally, in Fig. 3c we show the central longitudinal profile (y = 0) of Ln(T). Note the strong asymmetry of this profile in front of and behind the laser spot.

In the following we will propose three methods to measure the thermal diffusivity that are based on the analysis of the shape of the central transverse profile, the central longitudinal profile and the transverse parabolas. All of them lead to simple linear relations, which have the advantage of avoiding complex and delicate multiparametric fittings.

It is worth noting that, according to the relativity principle, the three methods are also valid in the experimental configuration where the sample remains at rest while the laser is moving at constant velocity along a straight line onto the sample surface. This is the so-called "flying spot" infrared thermography, which in recent years has raised the interest of the IR thermography community for quantitative characterization of large surfaces [10,11].

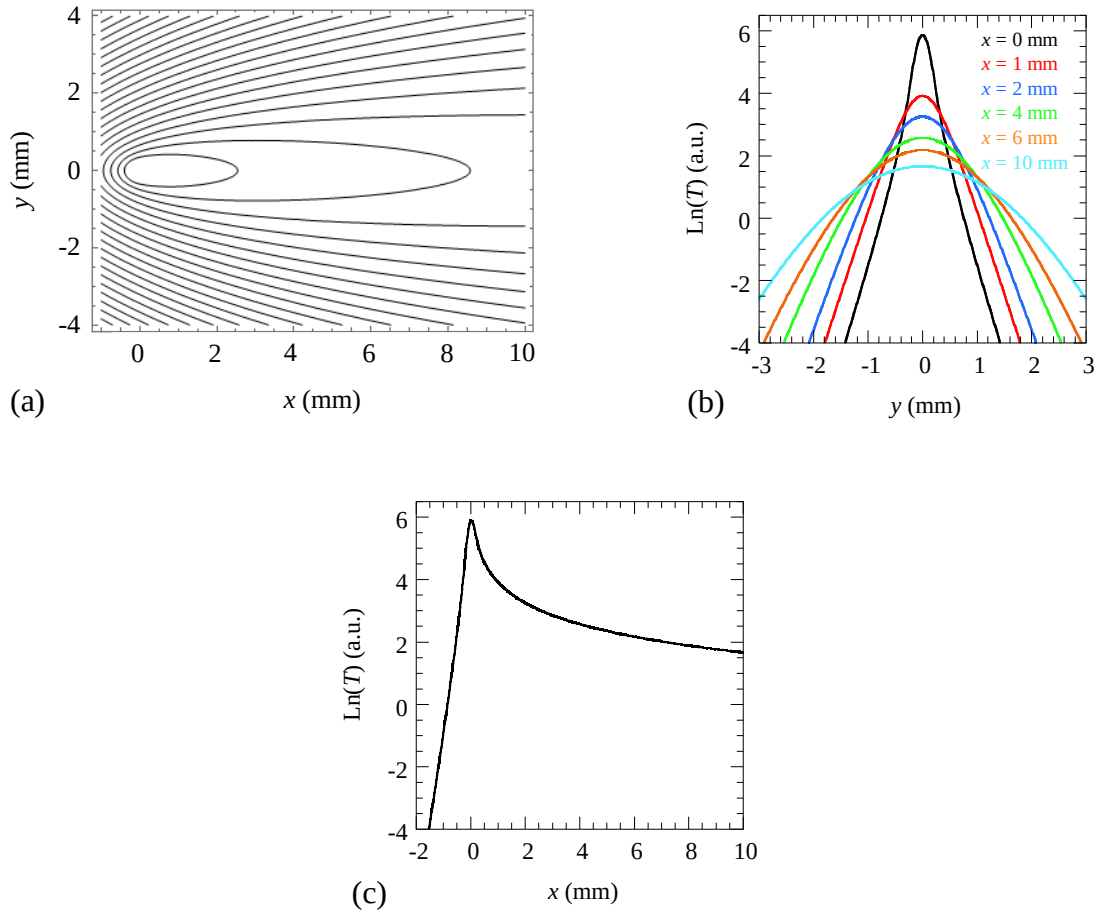

Fig. 3. (a) Calculations of the contour plots of the natural logarithm of the surface temperature for an anisotropic sample (D_x = 4 mm^2/s, D_y = 1 mm^2/s) heated by a 1 W laser beam of radius a = 0.2 mm and h = 0, when the steady-state has been stablished. The sample is moving at v = 2 cm/s. (b) Transverse profiles of Ln(T) at several longitudinal distances, x, from the laser spot. (c) Central longitudinal profile (y = 0) of Ln(T).

3.1 The "central transverse profile" method

Fig. 4a shows the calculations of the central (x = 0) transverse profile of the natural logarithm of the surface temperature using Eq. (3) for the same anisotropic sample as in Fig. 3, with a = 0 and in the absence of heat losses (h = 0). Two cases are considered. (a) If the material is opaque and thick, we have found that the natural logarithm of the temperature multiplied by the transverse distance, Ln(Ty), behaves linearly as a function of the transverse distance, y. (b)

If the material is an opaque and thin sample, or is transparent, the natural logarithm of the temperature multiplied by the square root of the transverse distance, $\mathrm{Ln}(Ty^{0.5})$, is a linear function of the transverse distance. The origin of the difference lies in the fact that the expression of the surface temperature for opaque and thick samples shows an additional $1/\sqrt{t}$ factor with respect to both opaque and thin and transparent samples, as can be observed in Eqs. (2). The slope (m) of these straight lines is related to the sample velocity and the transverse thermal diffusivity, D_y, through the simple formula:

$$m = \pm \frac{v}{2D_y}. \qquad (4)$$

In order to check the influence of heat losses on the central transverse profile, we have performed calculations for several values of the heat losses coefficient. Although realistic values of h at room temperature range from 6-10 $\mathrm{Wm^{-2}K^{-1}}$, we have checked that this profile remains unaffected for h values as high as 100 $\mathrm{Wm^{-2}K^{-1}}$. We have also analyzed the effect of the laser spot radius on the linear behavior of the central transverse profiles. In Fig. 4b we show Calculations performed for the same thermally thick material as in Fig. 4a. As can be observed, far away from the laser spot the linearity is kept with the same slope given by Eq. (4). This conclusion is also valid for opaque and thin or transparent samples. Accordingly, the thermal diffusivity along the transverse direction with respect to the sample movement can be obtained in a simple manner using Eq. (4).

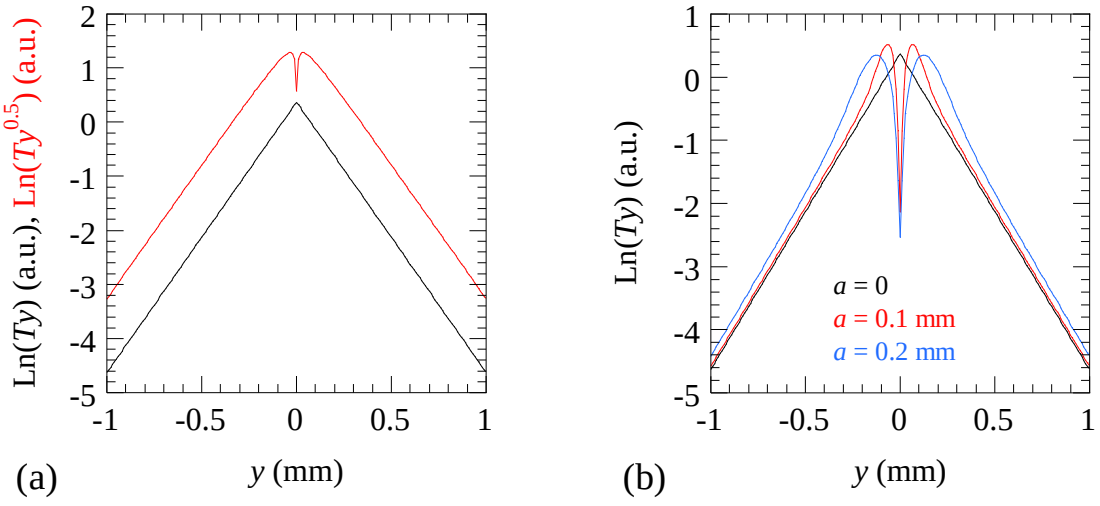

Fig. 4. (a) Calculations of the central transverse profile of $\mathrm{Ln}(Ty)$ for an opaque and thick sample (black curve) and $\mathrm{Ln}(Ty^{0.5})$ for an opaque and thin sample or a transparent sample (red curve). Calculations have been performed for the same anisotropic sample as in Fig. 3 with $a = 0$ and $h = 0$. (b) Effect of the laser spot radius on the central transverse profile for opaque and thick samples.

On the other hand, the linear behavior shown in Fig. 4a allows defining the thermal diffusion lengths (μ) along the transverse directions with respect to the laser movement as the distance with respect to the laser spot for which Ln(Ty) decreases by a factor e. This transverse thermal diffusion length is given by $\mu_i = 2D_i/v$, with $i = y$ and z. In particular, μ_z defines the depth penetration of the transient thermal energy in experiments with a moving sample. Accordingly, a sample behaves as thermally thick if its thickness $L > 2\mu_z$, while it behaves as thermally thin if $L < 0.5\mu_z$.

3.2 The "central longitudinal profile" method

Fig. 5a shows the calculations of the central ($y = 0$) longitudinal profile of the natural logarithm of the surface temperature using Eq. (3) for the same anisotropic sample as in Fig. 3, with $a = 0$ and $h = 0$. Unlike in the transverse profile there is no symmetry with respect to the laser position. For $x > 0$, the curve is flat and lacks information on the sample thermal diffusivity. For $x < 0$, there is a linear relation depending on the sample velocity and thermal diffusivity. As before, two cases are considered. (a) If the material is opaque and thick we have found that the natural logarithm of the temperature multiplied by the longitudinal distance, Ln(Tx), behaves linearly as a function of the longitudinal distance, x. (b) If the material is an opaque and thin sample, or is transparent, we have found that the natural logarithm of the temperature multiplied by the square root of the longitudinal distance, Ln($Tx^{0.5}$), is a linear function of the longitudinal distance. The slope (m) of these straight lines is related to the sample velocity and longitudinal thermal diffusivity, D_x, through the simple formula:

$$m = \frac{v}{D_x}. \qquad (5)$$

As in subsection 3.1, calculations performed for heat losses coefficients up to $h = 100$ $Wm^{-2}K^{-1}$ do not reveal any change in the slope of the straight line, indicating that "central longitudinal profile" method is not affected by heat losses. Moreover, the slope of the straight line is neither modified when considering realistic non-zero laser spot radii (see Fig. 5b). These evidences indicate that Eq. (5) provides a simple and robust method to retrieve the thermal diffusivity along the sample movement direction.

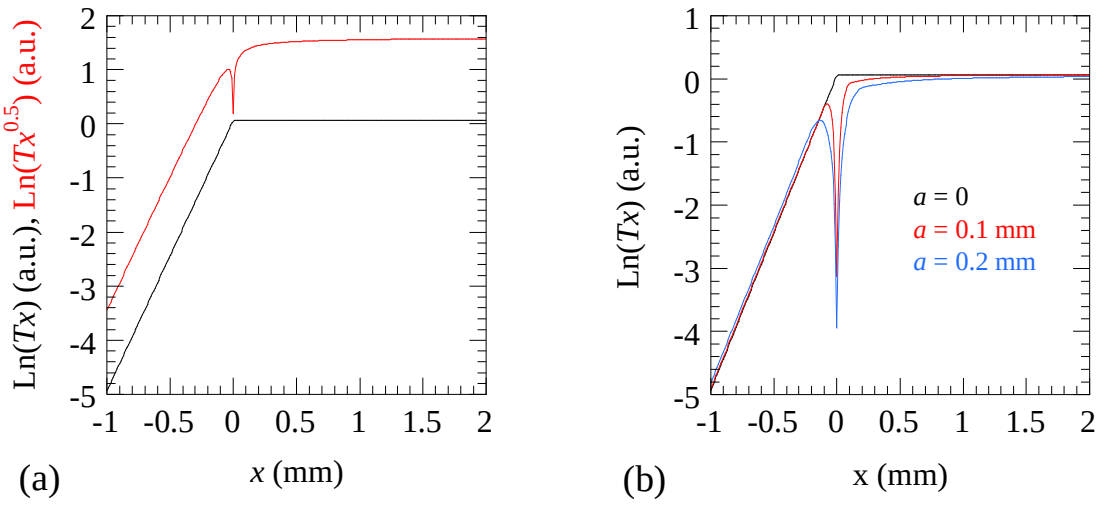

Fig. 5. (a) Calculations of the central longitudinal profile of Ln(Tx) for an opaque and thick sample (black curve) and Ln($Tx^{0.5}$) for an opaque and thin sample or a transparent sample (red curve). Calculations have been performed for the same anisotropic sample as in Fig. 3 with a = 0 and h = 0. (b) Effect of the laser spot radius on the central longitudinal profile.

As we did in the previous subsection, the linear behavior shown in Fig. 5a allows defining the thermal diffusion lengths along the longitudinal direction as the distance with respect to the laser spot for which Ln(Tx) decreases by a factor e. This longitudinal thermal diffusion length is given by $\mu_x = D_x / v$. Note that the depth penetration of heat in experiments with a moving sample is different in the longitudinal and transverse directions, even for isotropic samples.

3.3 The parabolas method

Eq. (1) gives the temperature field when the sample is heated by a brief laser pulse of Gaussian profile. According to these equations, the temperature along the x and y axes features Gaussian profiles for all times after the laser pulse and therefore the natural logarithm of the temperature profiles along the principal axes are parabolas

$$Ln\left[T(x,0,0,t)\right] = A(t) - C_x(t)x^2, \tag{6a}$$

$$Ln\left[T(0,y,0,t)\right] = A(t) - C_y(t)y^2, \tag{6b}$$

where the inverse of the second order coefficient of the parabolas is a linear function of time: $\frac{1}{C_j(t)} = \frac{a^2}{2} + 4D_j t$ with j = x and y. The slope (m_j) of this linear relation gives the thermal diffusivity: $m_j = 4D_j$. This "parabolas method", which we have checked is neither affected by heat losses for h < 100 $Wm^{-2}K^{-1}$, provides an efficient tool to measure the thermal diffusivity of isotropic and anisotropic solids [10]. As can be seen in Fig. 3b, the transverse profiles of Ln(T) become parabolas as going away from the laser spot. Moreover, numerical calculations performed varying D_x, D_y, a and v show that the inverse of the second order coefficient of those parabolas verifies the same linear relation as in static flash measurements

$$\frac{1}{C_y} = \frac{a^2}{2} + 4D_y t = \{x = vt\} = \frac{a^2}{2} + \frac{4D_y}{v} x \,. \tag{7}$$

This result indicates that the inverse of the second order coefficient of the parabolas is a linear function of the distance to the laser spot, whose slope equals:

$$m = \frac{4D_y}{v} \tag{8}$$

and the intercept is $a^2/2$. This linearity provides a versatile method to retrieve the transverse thermal diffusivity of a moving sample. It is worth noting that this result is valid for the three kind of materials analyzed in Eqs. (2), regardless the laser power and the sample effusivity. Moreover, although heat losses reduce the temperature rise of the sample, the coefficient of the second order of the parabolas remains unaffected.

In order for the method to be applied properly we need to establish when the lateral profiles of Ln(T) are parabolas satisfying Eq. (7). In Fig. 6 we show the comparison of the quasi-parabola obtained from Eq. (3) and the exact parabola given by Eq. (7). Calculations have been performed for the same anisotropic sample as before (D_x = 4 mm^2/s, D_y = 1 mm^2/s, ε_z = 3000 $Ws^{0.5}m^{-2}K^{-1}$), using the same experimental parameters (1 W laser beam with radius a = 0.2 mm, heat losses coefficient h = 0, velocity v = 2 cm/s and steady-state conditions). Two transverse profiles of Ln(T) are shown: one for x = 2 mm and the other one for x = 4 mm. The continuous lines correspond to the calculation of Eq. (3) and the dotted lines the calculations of Eq. (7). The residuals, i.e. the difference between both, are also shown. As can be observed, as x increases the residuals are reduced.

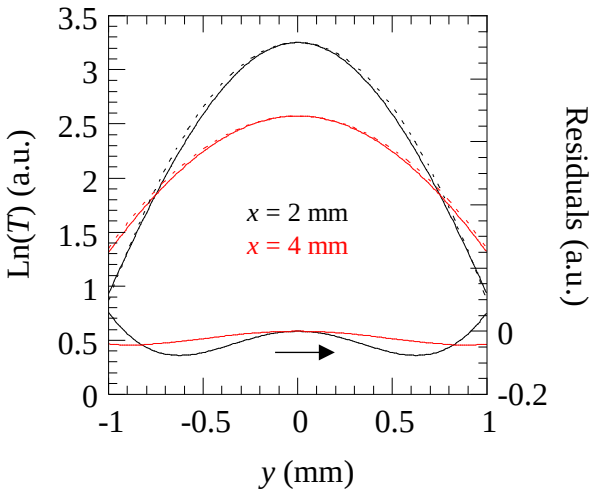

Fig. 6. Calculations of the transverse profiles of Ln(T) for the same anisotropic material and experimental parameters as in Fig. 3. Continuous lines correspond to the quasi-parabola given by Eq. (3) and the dotted lines to the exact parabola given by Eq. (7). The residuals, the difference between both, are also shown.

Now we want to determine the minimum distance from the laser spot, $x_{\min}$, for which the difference between the quasi-parabola given by Eq. (3) and the exact parabola given by Eq. (7) is negligible. Systematic numerical calculations performed by varying D and v indicate that if the Péclet number, Pe, equals

$$Pe = \frac{v x_{\min}}{D_x} \approx 20, \qquad (9)$$

the difference is less than 0.05. To visualize the consequences of this result let us consider a fixed sample velocity of 2 cm/s and two materials of extreme thermal properties: a typical polymer (D = 0.1 mm^2/s) and copper (D = 100 mm^2/s). According to Eq. (9), in the case of the polymer the minimum distance to the laser spot where the "parabolas method" can be applied is $x_{\min} \approx 0.1$ mm, whereas in the case of copper this limit rises up to $x_{\min} \approx 10$ cm. Consequently, when dealing with a good thermal conductor it is required to use a quite high sample velocity to keep $x_{\min}$ in the order of a few millimeters.

4. Experimental results and discussion

Figure 7 shows the scheme of the IR thermography setup, where the laser spot is kept fixed and the sample is moved at constant velocity. A CW laser (532 nm, up to 6 W) is focused

at the sample surface by means of a 10 cm focal length lens to a radius of about 200 μm. A Ge window, which reflects visible light and transmits IR wavelength, is used to prevent the scattered laser radiation from reaching the IR camera. A small mirror, glued to the Ge window, directs the laser beam onto the sample surface, perpendicularly. An IR video camera (FLIR, model SC7500, 320 × 256 pixels, pitch 30 μm and spectral band from 3 to 5 μm) records the temperature field at the sample surface. An IR microscope lens is used to improve the spatial resolution of the IR camera to 30 μm, with a field of view of 9.60 mm x 7.68 mm. The sample is mounted on a dynamic system (cart + track) that is coupled to an electric engine to move the cart at constant speed in the range between 0.5 and 15 cm/s.

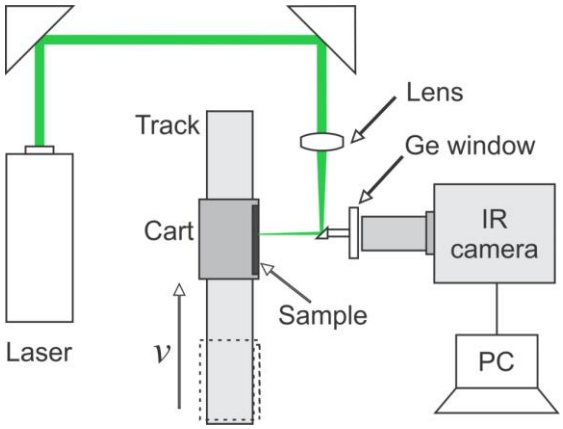

Figure 7: Scheme of the experimental setup with a moving sample and the laser spot at rest.

The speed of the sample is measured by counting the number of frames between the entrance and the exit of one end of the sample in the field of view of the camera and taking into account the length of the sample and the frame rate of the camera. In this way, the sample speed is measured with an uncertainty of less than 0.5%. We worked at the maximum frame rate allowed by the IR camera: 330 frames/s at full frame and up to 2000 frames/s applying a subwindowing (320 × 70 pixels). On the other hand, in order to enhance the signal to noise ratio, several hundred of thermograms are averaged after reaching the steady state. For a comparison, we show in Fig. 8 the single thermogram and the average thermogram corresponding to a stainless steel AISI-304 sample moving along the horizontal axis at 6 cm/s. This remarkable noise reduction will allow us to retrieve the sample thermal diffusivity with high accuracy.

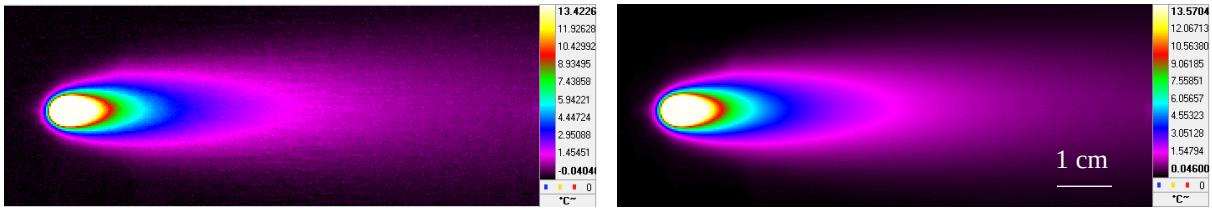

(a) (b)

Figure 8: (a) Single thermogram and (b) averaged thermogram over several hundreds of thermograms corresponding to an AISI-304 sample moving to the right at 6.0 cm/s.

To verify the validity of the three methods proposed in this work we have tested them on some calibrated samples covering a wide range of thermal diffusivity values, from thermal insulators (polymers) to good thermal conductors (metals): Polyether-ether-ketone (PEEK), AISI-304, Ni, Zn and Al 2024-T6 alloy. We have also measured the anisotropic thermal diffusivity of balsa wood. All these materials have been covered by a thin graphite layer to enhance both the absorption to the laser and the IR emissivity. We have also tested the method on two semitransparent samples: orange coloured Polymethyl-methacrylate (PMMA) and grey BK7 glass. Moreover, three thin samples have also been tested: 0.25 mm thick PEEK and 0.20 mm thick AISI-304 and Zn. Regarding the sample speed, for bad thermal conductors (polymers and glass) sample speeds in the lower range of our track, 1.5 - 2.5 cm/s, were used. Contrarily, for good thermal conductors higher speeds are better adapted: from 6 cm/s for AISI-304 up to 15 cm/s for Al alloy. As a rule of thumb, we can say that the most appropriate speed for thermal diffusivity measurements produces a thermogram with an aspect ratio of the pseudo-ellipses around 3:1, similar to that found in Fig. 8.

Figure 9 shows the transverse profiles of Ln(T) corresponding to the AISI-304 sample thermogram plotted in Fig. 8b. For the sake of clarity, only eight transverse profiles, separated by 1 mm, are shown. Dots are the experimental data and the continuous lines are the parabolic fits. As can be observed, the experimental profile at x = 1 mm, very close to the laser spot, differs from a parabola. Actually, according to Eq. (9), the minimum distance from the laser spot to fulfil a parabola is $x_{min} \approx 1.3$ mm. This means that only transverse profiles at distances larger than 1.3 mm will be used in the parabolas method. Figure 10 shows the inverse of the second order coefficient of the parabolas versus the longitudinal distance for some of the calibrated materials used in this work. Dots are the experimental data and the continuous lines are the linear fits. Figure 10a shows the results for thermal insulators, which are very clean and

Fig. 10b for good thermal conductors, for which the noise increases as the thermal diffusivity does. In fact we were unable to measure the thermal diffusivity of a copper sample due to the poor signal to noise ratio. Then, using Eq. (8) the thermal diffusivity is obtained. The results, summarized in Table 1, agree with the literature values and confirm the validity of the parabolas method. The uncertainty in the *D* values varies from less than 3% in thermal insulators up to 5-6% for good thermal conductors. It should be noted that, according to Eq. (7), the intercept of the linear fits in Fig. 10 gives the laser radius. Actually, for thermal insulators we obtain a laser radius in the range 0.2-0.3 mm, very close to the optically measured value. For good thermal conductors, instead, the accuracy is not good enough to estimate the laser radius.

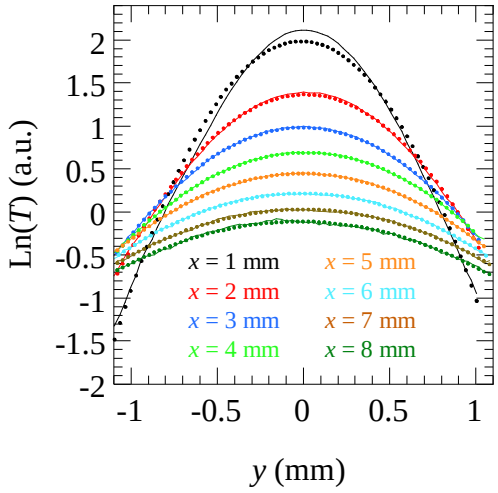

Figure 9: Transverse profiles of Ln(*T*) at eight distances from the laser spot centre (*x*) for the AISI-304 thermogram shown in Fig. 8b. Dots are the experimental data and the continuous lines are the parabolic fits.

We have also tested a piece of Balsa wood, which is a soft, low-density heterogeneous material. As its thermal transport properties are anisotropic, measurements have been performed in the direction perpendicular to the growth rings ($\perp$) and in the direction parallel ($\parallel$) to them. The retrieved values of the thermal diffusivity are given in Table 1. It is worth noting that for this heterogeneous material there are differences in the physical properties from tree to tree depending on the age, climate and moisture [13,14]. That is the reason for the large dispersion of the literature values given in Table 1. Anyway, a thermal anisotropy factor of 2.5, similar to that found in this work, has been already reported [15].

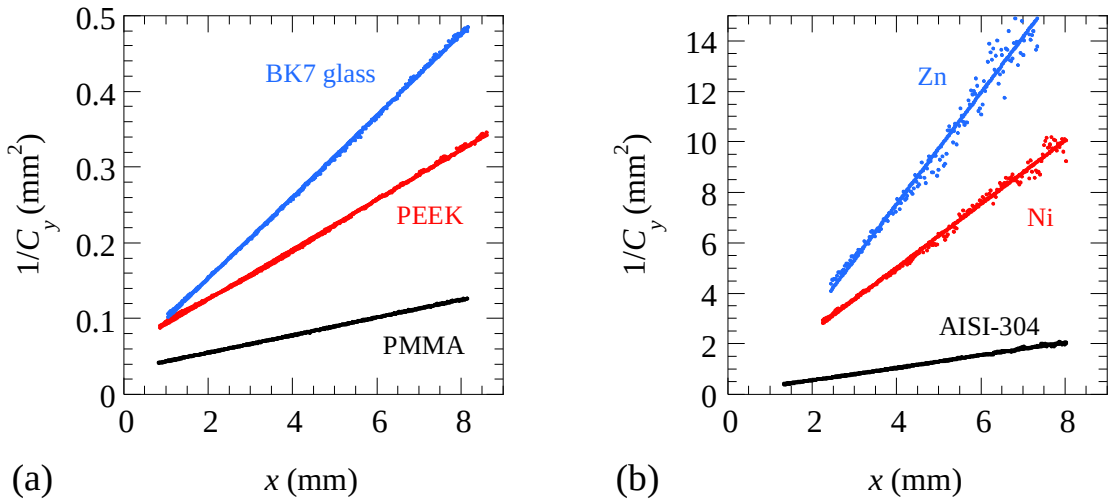

Figure 10: Inverse of the parabolic coefficient versus the longitudinal distance for some of the calibrated materials used in this work. Dots are the experimental data and the continuous lines are the linear fits. (a) Thermal insulators. (b) Good thermal conductors.

Then, we have tested the "central transverse profile" method. We have analysed the same averaged thermograms as those used for the parabolas method. Figure 11a shows the transverse profiles of Ln(Ty) for a thick Zn sample and of Ln($Ty^{0.5}$) for two thin plates (L = 0.2 mm) of Zn and AISI-304. Dots are the experimental data and the continuous lines are the linear fits. By applying Eq. (4), the transverse thermal diffusivity is obtained. The results, which agree with the literature values, are summarized in Table 1.

Finally, we have checked the "central longitudinal profile" method. Figure 11b shows the longitudinal profiles of Ln(Tx) and Ln($Tx^{0.5}$) for the same three samples as in Fig. 11a. Dots are the experimental data and the continuous lines are the linear fits. As predicted by the theory (see Fig. 5), for x > 0 there is a flat behaviour without any information on the thermal diffusivity. For x < 0 there is a linear relation whose slope gives the longitudinal thermal diffusivity by applying Eq. (5). The results are summarized in Table 1.

As can be observed in Table 1, no results are given for insulators using both central profiles methods. The reason for that is not a limitation of the method itself, but it is related to the lower velocity limit of our setup (1.5 cm/s). At this speed the number of points is too small to provide reliable thermal diffusivity values. For those materials either velocities of a few mm/s or a higher spatial resolution are needed.

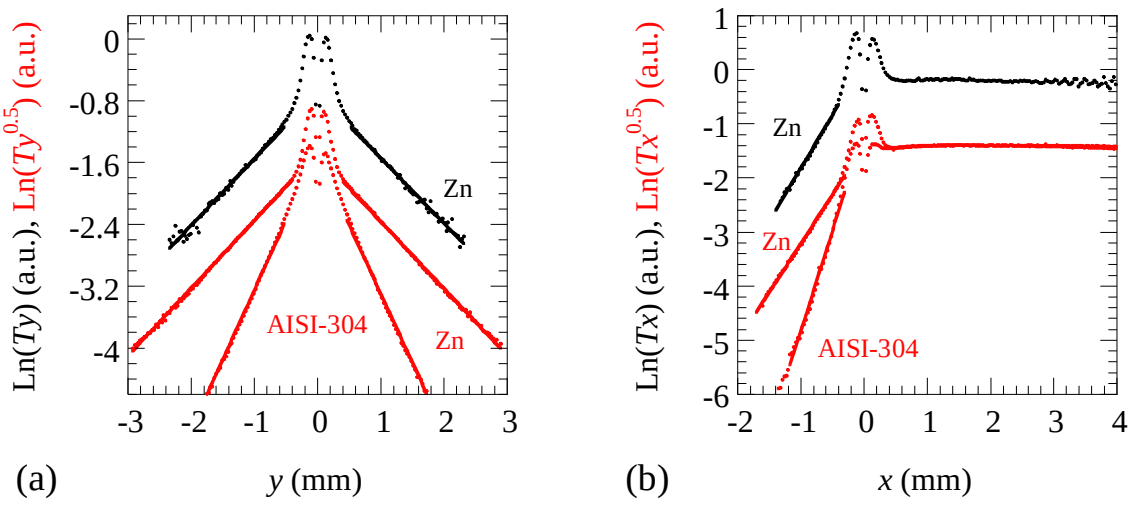

Figure 11: (a) Transverse profiles and (b) longitudinal profiles in natural logarithm scale for thick Zn (black curve) and for thin Zn (L = 0.2 mm) and AISI-304 (L = 0.2 mm) in red. Dots are the experimental data while the continuous lines are the linear fits.

Before concluding, let us remark some drawbacks of the methods proposed in this work. (a) On the one hand, they are valid for quite big samples, since the steady-state must have been reached. Anyway, as these methods are addressed to in-line production or in-line quality control processes, this is not a real limitation. (b) On the other hand, the two central profiles methods require a high spatial resolution to have enough experimental data to clearly define the linear region. Accordingly, IR cameras with high resolution (640 × 512 pixels or higher) and/or microscope lenses, leading to a spatial resolution better than 30 μm, are highly recommended. Note that the parabolas method does not suffer from this limitation, since even with few data the second order coefficient of the parabolas can be obtained accurately [20]. (c) Besides, the central profiles methods are not valid when the thermal thickness of the specimen is intermediate, i.e. neither thick nor thin. This issue can be overcome by selecting, whenever it is possible, the appropriate velocity range: increasing the speed for the sample to behave as thick or reducing it to approach the thermally thin limit. (d) One of the potential applications of these methods is to detect heterogeneities in-line production. This application requires local thermal diffusivity measurements methods. For this purpose, it is worth noting that the central profiles methods are preferable to the parabolas method since the former only requires taking temperature data a few millimetres around the laser spot, whereas the latter requires analysing the temperature along a centimetre or more in the direction of the sample movement.

5. Conclusion

In this paper we have proposed three methods to measure the in-plane thermal diffusivity of (an)isotropic solids moving at constant velocity, by analyzing the surface temperature field in logarithmic scale. These methods are based on simple linear relations, which avoid complex multiparametric fitting procedures. Moreover, they are valid not only for opaque samples, but also for semitransparent ones and they are not affected by heat losses by convection and radiation. The validity of the methods have been confirmed experimentally on calibrated samples covering a wide range of thermal diffusivities. It is worth noting that these methods can be directly applied when the sample is at rest while its surface is scanned by a laser spot moving at constant velocity, i.e. the classical Flying Spot infrared thermography.

Acknowledgments

This work has been supported by Ministerio de Economía y Competitividad (DPI2016-77719-R, AEI/FEDER, UE), by Universidad del País Vasco UPV/EHU (GIU16/33) and by Conacyt (Beca Mixta 2017 Movilidad en el extranjero).

Table 1. Retrieved thermal diffusivities (mm^2/s) using the three methods proposed in this manuscript. The uncertainty varies from less than 3% for thermal insulators up to 5-6% for good thermal conductors.

Sample	*D* (Parabolas method)	*D* (Transverse profile)	*D* (Longitudinal profile)	*D* (Literature)[13-19]
PEEK	0.19	-	-	0.18
AISI-304	4.0	4.0	4.1	4.0
Ni	21	22	20	22
Zn	43	43	40	42
Al 2024-T6	70	73	70	73
Balsa wood ∥	0.44	-	-	0.30-0.51
Balsa wood ⊥	0.22	-	-	0.14-0.25
Colored PMMA	0.12	-	-	0.11
BK7-glass	0.56	0.52	0.50	0.5-0.6
PEEK (L = 0.25 mm)	0.20	-	-	0.18
AISI-304 (L = 0.2 mm)	3.9	3.9	4.0	4.0
Ni (L = 0.2 mm)	-	20	20	22
Zn (L = 0.2 mm)	-	45	45	42

References

[1] A. Salazar, On thermal diffusivity, Eur. J. Phys. **24**, 351-358 (2003).

[2] B. Abad, D.A. Borca-Tasciuc, M.S. Martin-Gonzalez, Non-contact methods for thermal properties measurements, Renewable and Sustainable Energy Reviews **76**, 1348-1370 (2017).

[3] E.J. Kubiak, Infrared detection of fatigue cracks and other near-surface defects, Appl. Opt. **7**, 1743-1747 (1968).

[4] J.C. Krapez, Résolution spatiale de la camera thermique à source volante, Int. J. Therm. Sci. **38**, 769-779 (1999).

[5] J. Schlichting, M. Ziegler, A. Dey, Ch. Maierhofer and M. Kreutzbruck, Efficient data evaluation for thermographic crack detection, QIRT J. **8**, 119-123 (2011).

[6] S.E. Burrows, S. Dixon, S.G. Pickering, T. Li and D.P. Almond, Thermographic detection of surface breaking defects using a scanning laser source, NDT&E Int. **44**, 589-596 (2011).

[7] T. Maffren, P. Juncar, F. Lepoutre and G. Deban, Crack detection in high-pressure rurbine blades with flying spot active thermography in the SWIR range, Rev. Progress Quantitative Nondestructive Evaluation, AIP Conference Proc. **1430**, 515-522 (2012).

[8] A. Thiam, J.C. Kneip, E. Cicala, Y. Caulier, J.M. Jouvard and S. Mattei, Modeling and optimization of open crack detection by flying spot thermography, NDT&E Int. **89**, 67-73 (2017).

[9] C. Boué and S. Holé, Open crack depth sizing by multi-speed continuous laser stimulated lock-in thermography, Meas. Sci. Technol. **28**, 065901 (2017).

[10] L. Gaverina, J.C. Batsale, A. Sommier and C. Pradere, Pulsed flying spot with the logarithmic parabolas method for the estimation of in-plane thermal diffusivity fields on heterogeneous and anisotropic materials, J. Appl. Phys. **121**, 115105 (2017).

[11] L. Gaverina, A. Sommier, J.L. Battaglia, J.C. Batsale and C. Pradere, Pulsed flying spot elliptic method for the estimation of the thermal diffusivity field of orthotropic materials, Int. J. Therm. Sci. 1**25**, 142-148 (2018).

[12] N.W. Pech-May, A. Mendioroz and A. Salazar, Simultaneous measurement of the in-plane and in-depth thermal diffusivity of solids using pulsed infrared thermography with focused illumination, NDT&E International **77**, 28-34 (2016).

[13] N.J. Kotlarewski, B. Ozarska and B.K. Gusamo, Thermal conductivity of Papua New Guinea balsa wood measured using the needle probe procedure, Bioresources **9**, 5784-5793 (2014).

[14] R. Hrčka, Variation of thermal properties of beech wood in the radial direction with moisture content and density, in Wood Structure and Properties 10, Ed. J. Kúdela and R. Lagana, Arbora Publishers, Zvolen, Slovakia, 2010. p. 111-116.

[15] P.Niemz, W. Sonderegger and S. Hering, Thermal conductivity of Norway spruce and European beech in the anatomical directions, Annals of Warsaw University of Life Sciences, Forestry and Wood Technology **72**, 66-72 (2010).

[16] Y.A. Çengel, Heat Transfer: A practical Approach, McGraw-Hill, Boston, (2003).

[17] Goodfellow catalogue at http://www.goodfellow.com.

[18] D.P. Almond and P.M. Patel, Photothermal Science and Techniques, Chapman & Hall, London (1996), p. 16,17.

[19] L.R. Touloukian, R.W. Powell, C.Y. Ho and M.C. Nicolasu, *Thermal Diffusivity* (IFI/Plenum, New York, 1973).

[20] L. Gaverina, M. Bensalem, A. Bedoya, J. González, A. Sommier, J.L. Battaglia, A. Salazar, A. Mendioroz, A. Oleaga, J.C. Batsale and C. Pradere, Constant Velocity Flying Spot for the estimation of in-plane thermal diffusivity on anisotropic materials (to be published).